Human aB-crystallin discriminates between aggregation-prone and function-preserving variants of a client protein

Marc Sprague-Piercy[†], **Eric Wong**[‡], **Kyle W. Roskamp**[‡], **Joseph Fakhoury**[‡], **J. Alfredo Freites**[‡], **Douglas J. Tobias**[‡], **Rachel W. Martin**[‡,¶]

[†]Department of Molecular Biology and Biochemistry, University of California, Irvine CA 92697

[‡]Department of Chemistry, UC Irvine, Irvine, CA 92697-2025

[¶]Department of Molecular Biology and Biochemistry, UC Irvine, Irvine CA 92697

Abstract

Background—The eye lens crystallins are highly soluble proteins that are required to last the lifespan of an organism due to low protein turnover in the lens. Crystallin aggregation leads to formation of light-scattering aggregates known as cataract. The G18V mutation of human γS-crystallin, which is associated with childhood-onset cataract, causes structural changes throughout the N-terminal domain and increases aggregation propensity. The holdase chaperone protein aB-crystallin does not interact with wild-type γS-crystallin, but does bind its G18V variant (γS-G18V). The specific molecular determinants of aB-crystallin binding to client proteins is incompletely charcterized. Here, a new variant of γS, γS-G18A, was created to test the limits of aB-crystallin selectivity.

Methods—Molecular dynamics simulations were used to investigate the structure and dynamics of γS-G18A. The overall fold of γS-G18A was assessed by circular dichroism (CD) spectroscopy and intrinsic tryptophan fluorescence. Its thermal unfolding temperature and aggregation propensity were characterized by CD and DLS, respectively. Solution-state NMR was used to characterize interactions between aB-crystallin and γS-G18A.

Results—γS-G18A exhibits minimal structural changes, but has compromised thermal stability relative to γS-WT. The placement of alanine, rather than valine, at this highly conserved glycine position produces minor changes in hydrophobic surface exposure. However, human aB-crystallin does not bind the G18A variant, in contrast to previous observations for γS-G18V, which aggregates at physiological temperature.

Conclusions—aB-crystallin is capable of distinguishing between aggregation-prone and function-preserving variants, and recognizing the transient unfolding or minor conformers that lead to aggregation in the disease-related variant.

General Significance—Human aB-crystallin distinguishes between highly similar variants of a structural crystallin, binding the cataract-related γS-G18V variant, but not the function-preserving γS-G18A variant, which is monomeric at physiological temperature.

dtobias@uci.edu.

Introduction

For many proteins, the solubility and oligomerization state are critical functional properties that are subject to alteration by mutation or post-translational modification. Protein aggregation is associated with many human pathologies, including Alzheimer's and Parkinson's diseases as well as chronic respiratory conditions,[1] transthyretin amyloidosis,[2] and sickle cell anemia.[3] Protein aggregates can cause disease via loss of function, as in α-antitrypsin deficiency: when α-antitrypsin aggregates, the normal function of this protein to inhibit proteolysis is lost, leading to tissue disruptions.[1] In other cases pathogenesis is due to direct cytotoxicity of the aggregates, as in transthyretin amyloidosis.[2]

In the case of crystallins, their normal function is to maintain lens refractivity and transparency. These proteins are therefore exceptionally stable and soluble, even at high concentrations (above 400 mg/mL in humans).[4,5] In the eye lens there is a negligible amount of protein turnover,[6] meaning that the crystallins must remain soluble throughout the life of an organism, offering a unique model for the study of protein stability and solubility. With age, however, accumulated damage to the crystallins results in light-scattering aggregates causing an opacification of the lens, a condition known as cataract.

There are two main classes of lens crystallins, α- and $\beta\gamma$-crystallins. The α-crystallins are small holdase chaperone proteins that form very large, multimeric complexes.[7,8] The $\beta\gamma$-crystallins are highly refractive structural proteins that maintain the refractive index gradient of the eye lens. Post-translational modifications including deamidation,[9] glycation,[10] and UV-filter adduction[11] have been shown to reduce crystallin solubility. Many mutations in both α- and $\beta\gamma$-crystallins have been associated with early-onset cataract, including the R116C[12] and the R49C variants[13] of αA-crystallin, the R120G variant of αB-crystallin,[14] the S39C[15] variant of γS-crystallin, and the P23T[16–18] variant of γD-crystallin. In particular, the γS-G18V variant of γS-crystallin has been associated with childhood-onset cataract.[19]

The structure of γS-crystallin is typical of $\beta\gamma$-crystallins in general, with two double Greek key domains. Although the sequences of these two domains are not identical, their structures are very similar, resulting in a highly symmetric protein. A theme that has emerged from investigation of cataract-associated variants of γD- and γS-crystallin is their structures are often not dramatically different from that of the wild-type protein. In the V24M variant, the core of the N-terminal domain is more closely packed, but the protein maintains the overall β-sheet structure.[20] Similarly, the tertiary structures of the γS-D26G[21] and γS-G18V[22] variants are only subtly different from that of γS-WT. The structure of γS-crystallin with important features labeled is shown in Figure 1.

Although the structures of γS-G18V and γS-WT γS-crystallin are very similar, the holdase chaperone αB crystallin recognizes these subtle changes in structure, preferentially binding to the partially destabilized γS-G18V variant but not the wild-type protein.[22] The unfolding temperature of γS-G18V is 6 °C higher than the aggregation temperature, indicating that the aggregation of the protein is not due to the protein simply unfolding;[23] instead γS-G18V exhibits a slightly destabilized N-terminal domain characterized by an increase in

hydrophobic exposure on the surface of the protein.[24] Not all of the known cataract-associated variants of structural lens crystallins exhibit increased hydrophobic surface area or recognition by αB-crystallin. For instance, the cataract-associated I4F and V76D variants of γD-crystallin do not bind to αB to any appreciable degree, even though these variants are noticeably destabilized relative to γD-WT.[25]

In order to investigate which local changes in structural crystallins enable recognition by αB-crystallin, we generated the novel G18A variant of γS-crystallin (γS-G18A). This variant was chosen to provide a minimal structural disruption that may or may not be recognized by αB-crystallin, as the mutated residue is located in a tight turn with backbone torsion angles that are canonically favorable only for glycine. We find that although γS-G18A is thermally destabilized and somewhat aggregation-prone relative to γS-WT, it exhibits minimal structural perturbations at physiological temperature and is not recognized by αB-crystallin.

Results and discussion

Experiments and molecular dynamics simulations suggest that the overall fold of γS-G18A is similar to that of γS-WT

The circular dichroism (CD) spectra of γS-WT, γS-G18A, and γS-G18V were measured to probe changes in secondary structure. The spectrum of γS-G18A exhibits a minimum at 218 nm, indicative of a primarily β-sheet structure (Fig. 2A). The spectrum of γS-G18A is more similar to γS-WT than γS-G18V; it lacks the shoulder at 200–210 nm observed in the spectrum of γS-G18V.[19,23]

In vertebrate lens γ-crystallins, two buried tryptophans are ubiquitously conserved within each domain.[26,27] Each set acts independently as a FRET pair, enabling the γ-crystallins to quench UV radiation and act as a photoprotectant.[28,29] Minor changes to the chemical environment surrounding the tryptophans reduce their quenching efficiency, providing a sensitive measure to detect minor conformational changes.[30,31] Increased polarity of the tryptophan environment from solvent exposure results in red-shifting of the fluorescence spectrum.[32] This change can be observed for γS-G18V, in which the fluorescence is broadened and the peak intensity is red-shifted to 328 nm (Fig. 2B). The emission spectrum of γS-G18A is almost identical to that of γS-WT, consistent with the absence of increased relative solvent accessibility (RSA) observed in the γS-G18A Molecular Dynamics (MD) simulations (see below), and indicates that the chemical environments near the buried tryptophans are minimally perturbed (Supplementary Figure S1).

Anilinonaphthalene 8-sulfonate (ANS) is a small-molecule fluorophore often used to investigate hydrophobic surface exposure in proteins.[33,34] Binding is mediated through both hydrophobic and electrostatic interactions.[35,36] Increased hydrophobic surface area is observed in some cataract-related variants such as γS-G18V,[24] γS-V42M, and γD-P23T, but not others, including γS-D26G.[20,21,34] ANS fluorescence increases moderately in the presence of γS-G18A relative to γS-WT, but the signal is dramatically weaker than for γS-G18V (Fig. 2C). Similarly, a hypsochromic shift to 513 nm (from 525 nm) is observed for γS-G18A compared to 495 nm for γS-G18V. These changes indicate that γS-G18A exhibits

a small increase in hydrophobic surface area relative to γS-WT. We hypothesize that these changes are localized close to the mutation site; in our previous study of G18V the area around this loop opened up to expose more hydrophobic side-chains to solvent.[24] Further, the strong hypsochromic shifting in conjunction with increased fluorescence suggests strong interactions with positively charged residues, such as Arg19 and Arg20.

MD simulations of γS-WT and γS-G18A were performed to investigate mutation-induced changes in protein structure and dynamics. No dramatic changes were observed in the N-terminal domain (NTD) or C-terminal domain (CTD) of γS-WT or γS-G18A as a whole based on C_α root mean square deviation (RMSD). Whole-protein changes are attributable to the flexible N-terminal tail extension and inter-domain linker regions of the protein (Fig. 3). At the residue level, γS-G18A exhibits increased root mean-square fluctuations (RMSFs) within the α-helices and sequential loop sequences of the NTD (Supplementary Figure S2). Spatially, these regions are adjacent to the first β-hairpin, which contains residue 18. At the mutation site, no large changes in RMSF are observed. There is no increase in calculated solvent accessibility suggesting that the core of the protein would not be exposed and there would be no additional hydrophobic patches in γS-G18A when compared to WT (Supplementary Figure S1). The ψ backbone angle of A18 is identical to that of G18, whereas the φ angle is slightly larger and more broadly distributed (Fig. 4). Although it is difficult to determine the exact significance of this change, alanine and valine exhibit a near identical distribution of ψ-φ torsion angles in lens β- and γ-crystallins (Supplementary Figure S3). Like V18 of γS-G18V, the torsion angle of A18 is dissimilar to all native β- and γ-crystallin alanines. Therefore, even though it is not as bulky or hydrophobic, alanine may be expected to cause similar changes in the protein backbone conformation at the mutation site. In γS-G18V the torsion angle changes results in altered backbone hydrogen bonding with the subsequent β-strand relative to wild-type. This change, however, is not observed for γ-G18A. The absence of significant structural differences between γS-G18A and γS-WT as observed in the MD simulations does not necessarily preclude the possibility of increased aggregation propensity or α-crystallin binding, as it is well-established that structural changes to the lens γ-crystallins are not necessary to alter protein stability and aggregation in the lens. [18,20,21,23]

NMR chemical shifts of γS-G18A indicate only mild structural perturbations

The ^{1}H-^{15}N-HSQC[37] spectrum of γS-G18A (Fig. 5A) was measured in order to compare the NMR chemical shifts, a sensitive probe of the local chemical environment, to those of γS-WT and γS-G18V, which were measured previously. Chemical shift assignments were determined by comparison to the γS-WT and γS-G18V assignments from the BioMagResBank (BMRB) (Entries 17576 and 17582), in which 72 % of shifts were assigned. As a whole, the chemical shift perturbations (CSP) for γS-G18A indicate that the structure is much more similar to γS-WT than γS-G18V (Fig. 5B,C). The most pronounced differences are observed in the first 50 residues of the N-terminal domain. Even for these residues, the γS-G18A chemical shifts are still more similar to γS-WT than to γS-G18V. Residues 17-20 were not assignable, probably due to local structural rearrangement.

γS-G18A is of intermediate stability and aggregation propensity, between γS-WT and γS-G18V

The stability of γS-G18A relative to γS-WT and γS-G18V was measured in response to chemical stress. Chemical denaturation was performed using guanidine hydrochloride and assessed using the 355/325 nm fluorescence ratio (Fig. 6A). γS-WT and γS-G18A follow a two-state unfolding model with near identical unfolding midpoints at 2.1 M. In γS-G18V, three state-unfolding is observed with an unfolding intermediate between ~1 M and 2 M. The unfolding midpoint leading up to the intermediate is at 0.9 M and leading up to complete unfolding is 2.3 M. We hypothesize that γS-G18A does not exhibit an intermediate unfolding state because the minimal structural changes near the mutation site are not sufficient to catalyze unfolding of the N-terminal domain. This is corroborated by the "m" parameter for each protein, which is the dependance of G on concentration of denaturant. For the first transition observed in γS-G18V, m is higher than any slope in the second transition suggesting that some part of the protein is more suseptible to denaturation by guanidine hydrochloride. The δG_{app} of unfolding (Table 1) for each protein was calculated by using a linear approximation of a two-state unfolding curve as previously described.[39] γS-G18V was separated into two, two-state unfolding curves to generate its thermodynamic properties. G_{app} of unfolding was estimated by extrapolating a line of best fit for each data set to 0[39] (Supplementary Figure S4).

Thermal denaturation as measured by circular dichroism (CD) as a function of temperature (Fig. 6B). As previously observed, γS-WT is highly stable, with a unfolding midpoint at 77.67±0.03 °C whereas γS-G18V has the lowest unfolding midpoint at 66.74±0.04 °C. γS-G18A is of intermediate stability, with a unfolding midpoint at 69.87±0.05 °C. Although γS-G18A is nearly as robust as γS-WT with respect to chemical denaturation, its thermal stability of γS-G18A is noticably depressed.

Although γS-crystallin has a high thermal unfolding midpoint, thermal aggregation occurs at much lower temperatures, probably due to transiently unfolded states. Using dynamic light scattering (DLS), we measured protein aggregation as a function of temperature to investigate the behavior of γS-G18A (Fig. 6C). Between 44 °C and 47 °C, aggregates   10 nm in diameter are observable. These aggregates exceed 20 nm by 53 °C, after which large, insoluble aggregates   1000 nm are observed. The formation of intermediate size aggregates of γS-G18A is similar to that of γS-G18V, but at elevated temperature. In contrast, γS-WT does not exhibit any aggregation until 51–53 °C, when large, insoluble aggregates rapidly form. The similarity in thermal unfolding and aggregation of γS-G18A to γS-G18V suggests that γS-G18A has a similar aggregation pathway to γS-G18V, but shifted such that its onset occurs above physiological temperature.

αB-crystallin does not bind γS-G18A

Our characterization of γS-G18A indicates that protein stability is reduced compared to γS-WT, however, not as dramatically as it is in γS-G18V. Similarly, the aggregation propensity is intermediate, with an onset temperature around 45 °C. Moreover, γS-G18A does not appear to undergo large structural changes and does not exhibit a large increase in hydrophobic surface exposure. We next investigated how γS-G18A would interact with αB-

crystallin to learn more about how mutated, but essentially structurally unmodified, γ-crystallins behave as client proteins. Specifically, the objective was to determine whether the holdase chaperone aB-crystallin could discriminate between γS-G18A and γS-G18V. To this end, ^{1}H-^{15}N-HSQC experiments were performed using mixed samples of ^{15}N-labeled γS-G18A and natural abundance human aB-crystallin.

aB-crystallin forms high-molecular weight complexes that enable it to keep bound client proteins soluble.[8] Therefore, if aB-crystallin were able to recognize and bind γS-G18A, then the NMR spectra of the latter should display an increase in line-width and a change in chemical shift for residues that participate in binding to aB-crystallin, as previously observed for γS-G18V.[22] The HSQC spectra (Fig. 7A) of ^{15}N-labeled γS-G18A in the presence of natural abundance aB do not exhibit these changes, instead showing only modest chemical shift perturbations (Fig. 7B) compared with γS-G18A alone, even as temperature increases. The vast majority of the residues have a CSP of less than 0.05 ppm at both 25 (Fig. 7C) and 37 °C (Fig. 7D). Using a threshold of 2*RMS, the CSP of only 3 residues at 25 °C and only 4 residues at 37 °C are large enough to suggest significant conformational change. In both cases these residues with the highest CSP are in the NTD suggesting that there might be some very weak and transient interaction between the NTD of γS-G18A and aB-crystallin.

When comparing the NMR solved structure of γS-WT to the NMR structure of γS-G18V and the predicted structure of γS-G18A there are some key structural differences that could account for the changes in solubility and aB-crystallin selectivity (Fig. 8). It has been previously shown that the binding interface for aB-crystallin includes the 3 cysteine residues on γS-G18V.[24] In this regard γS-G18A is much more similar to γS-WT (Fig. 8A), so it is possible that the conformation of this region of γS-G18A does not promote interactions with aB-crystallin, while the altered conformation seen in γS-G18V does (Fig. 8B).

Conclusion

CD spectra and NMR chemical shifts suggest that the structure of γS-G18A is much more similar to γS-WT than to γS-G18V. However, the protein is thermally sensitive and there was a noticeable increase in aggregation propensity upon heating. Although it might be expected that a protein of intermediate aggregation potential between γS-WT and γS-G18V would also bind aB-crystallin to some degree, this is not the case for γS-G18A. This indicates that aB-crystallin is capable of discriminating very subtle structural changes in its client proteins, binding to the aggregation-prone G18V variant while leaving the function-preserving G18A variant untouched.

Materials and Methods

Protein expression and purification

The G18A variant of human γS-crystallin was generated using standard site directed mutagenesis. The cDNA encoding each protein and containing an N-terminal 6x-His tag was ligated into a pET28a(+) vector (Novagen, Darmstadt, Germany) and transformed into Rosetta *E. coli* for expression. All natural abundance proteins were expressed via β-D-1-

thiogalactopyranoside induction. A culture of Lysogeny broth (LB) was an inoculated from a starter culture at OD_{600} of ~0.05 and grown to an OD_{600} of ~1. The growth culture was grown at 37 °C to an OD_{600} of ~1.2 and then induced with 0.5 mM IPTG. After 24 hours at 25 °C the cells were harvested via centrifugation at 4000 rpm. The cells were lysed by sonication and subsequently centrifuged. The lysate supernatant was purified by nickel affinity chromatography and digested using TEV protease (produced in house) to remove the 6x His tag. The TEV protease and 6x His tag were removed by a second round of nickel affinity chromatography. Finally, size exclusion chromatography using a Superdex-75 SEC column was run to confirm purity. Protein masses were further confirmed using a Waters Xevo XS-QTOF.

For ^{15}N-labeled protein expression, a culture of *E. coli* in natural abundance LB was grown to an OD_{600} of ~1.2. The culture was spun down and the pelleted cells were resuspended in an equivalent volume of M9 minimal media. The culture was allowed to grow for 1 h at 16 °C and before being induced with β-D-1-thiogalactopyranoside at a final concentration of 0.5 mM. The cells were then grown at 18 °C for 36 hours. Purification was performed using the same procedure as the unlabeled abundance protein.

ANS Fluorescence

γS-WT, γS-G18V, and γS-G18A samples at 1 mg/mL (10 mM sodium phosphate, pH 6.9) were incubated with 750 μM of 1-Anilinonaphthalene-8-Sulfonic Acid (ANS) for 1 hour at room temperature. Spectra from 450–500 nm were collected on a Cary Eclipse Fluorescence Spectrophotometer (Agilent Technology Inc., Santa Clara California, USA) using a 390 nm excitation and 5 nm slit widths.

Circular dichroism (CD) and thermal unfolding

The circular dichroism of all proteins were collected using a J-810 spectropolarimeter (JASCO, Easton MD). Samples were prepared at 0.1 mg/mL (10 mM sodium phosphate, pH 6.9) and measured over the 190–250 nm wavelength range at RT. Thermal denaturing of proteins was assessed via the absorbance at 218.0 nm. A temperature ramp of 2 °C/min was applied over the temperature range of 25–85 °C using 5 second equilibrations and 1 °C increments. Thermal denaturation experiments were performed at a sample concentration of 0.25 mg/mL (10 mM sodium phosphate, 150 mM NaCl, 1 mM DTT, pH 6.9). The 50% unfolding point was calculated by fitting each curve to a two-state unfolding model as described previously.[23]

Tryptophan fluorescence and chemical unfolding

The intrinsic tryptophan fluorescence of all proteins was measured using a SpectraMax GeminiEM spectrometer (Molecular Devices, USA). Samples were excited at 295 nm and emission intensity was recorded from 300–400 nm. All samples were prepared at 0.1 mg/mL in 10 mM sodium phosphate, 50 mM sodium chloride, 0.05% sodium azide, pH 6.9.

The chemical unfolding via guanidine hydrochloride were assessed by 355/325 fluorescence ratio. Protein samples at 0.1 mg/mL were prepared in increasing concentrations of guanidine hydrochloride up to 6 M. The reaction mixtures were equilibrated at room temperature for

48 hours. Unfolding curves were generated by calculating the fluorescence ratio of 355 nm to 325 nm.

Dynamic light scattering

Protein thermal aggregation was measured via dynamic light scattering (DLS) using a Zetasizer Nano-ZS (Malvern Analytical, Malvern, United Kingdom). The number mean was used to assess particle sizes across a temperature range of 25–80 °C. Protein was diluted to 1 mg/mL in 10 mM sodium phosphate, 0.05% sodium azide, pH 6.9.

Solution-state NMR

^{15}N-HSQC experiments were conducted using an ^{1}H-^{13}C-^{15}N 5 mm tri-axis PFG triple resonance probe attached to a Varian ^{textitUnity}INOVA spectrometer (Agilent Technologies) operating at 800 MHz (Oxford Instruments). Proteins were concentrated to 35 mg/mL and then supplemented with 2mM TMSP and 10% D$_2$O. ^{1}H chemical shifts were referenced to TMSP and ^{15}N shifts were referenced indirectly to TMSP. NMR data were processed using NMRPipe[40] and analyzed using NMRFAM-Sparky.[41]

αB-crystallin binding assay

Lyophilized αB-crystallin was resuspended in 10 mM sodium phosphate at pH 6.9 and mixed in a 2:1 ratio with the ^{15}N-labeled γS-G18A variant of γS-crystallin at a concentration of 1.5 mM. A series of ^{15}N-HSQC experiments were then performed at 25, 27, 30, 32, 35, and 37 °C. The sample was incubated at the experimental temperature for 1 hour and the ^{15}N-HSQC experiment was run for 2 hours at each temperature. The chemical shifts collected were compared to a sample of a ^{15}N-labeled γS-G18A variant of γS-crystallin at a concentration of 1.5 mM. Chemical shift perturbations (CSP) were calculated using the following formula:

$$\Delta\delta_{avg} = \sqrt{\frac{(\Delta\delta_N/5)^2 + (\Delta\delta_H)^2}{2}}$$

Molecular dynamics simulations

The top configuration of the human γS-crystallin solution-state NMR structure[22] (PDB ID 2M3T) was used as the initial protein configuration in the γS-WT simulation and in the γS-G18A simulation after performing the Gly to Ala substitution at residue 18. The γS-WT simulation system consisted of a single protein chain, 11,493 water molecules and a single sodium counterion to neutralize the protein net charge for a total of 37,347 atoms. The initial simulation cell size was $63.573 \times 81.480 \times 77.315$ Å^3. The γS-G18A simulation system consisted of a single protein chain, 12,860 water molecules and a single sodium counterion for a total of 41,451 atoms. The initial simulation cell size was $81.52 \times 67.71 \times 80.34$ Å^3.

The simulations were performed with NAMD 2.9.[42] Each simulation system was subjected to 10,000 steps of conjugate-gradient energy minimization followed by a 1-ns MD run at constant pressure (1 bar) and a constant temperature (300 K) over which the protein was released from its initial configuration in a stepwise manner using harmonic restraints on all

backbone heavy atoms. The simulations were then run for 518 ns (γS-WT) and 1048 ns (γS-G18A) at constant temperature (300 K) and pressure (1 bar). The CHARMM36 force field[43–45] was used for proteins and ions and the TIP3P[46] model was used for waters. The smooth particle mesh Ewald method[47,48] was used to calculate electrostatic interactions. Short-range, real-space interactions were cut off at 12 Å by means of a switching function. A reversible, multiple time-step algorithm[49] was used to integrate the equations of motion with a time step of 4 fs for electrostatic forces, 2 fs for short-range nonbonded forces. The integration time step for bonded forces was 1 fs in the γS-WT simulation an 2 fs in the γS-G18A simulations . All bond lengths involving hydrogen atoms were held fixed using the SHAKE[50] and SETTLE[51] algorithms. A Langevin dynamics scheme was used for temperature control, and a Nosé-Hoover-Langevin piston was used for pressure control.[52,53]

Ramachandran analysis

The observed phi and psi angles for glycine, alanine, and valine were determined by collecting all available native vertebrate lens $\beta\gamma$-crystallins from the PDB (40 structures). Angles were calculated by using the DSSP package and processed using R.[54,55]

Supplementary Material

Refer to Web version on PubMed Central for supplementary material.

Acknowledgement

References

(1). Lomas D; Parfrey H A1-Antitrypsin Deficiency • 4: Molecular Pathophysiology. Thorax 2004, 59, 529–535. [PubMed: 15170041]

(2). Ruberg FL; Berk JL Transthyretin (TTR) Cardiac Amyloidosis. Circulation 2012, 126, 1286–1300. [PubMed: 22949539]

(3). Roseff SD Sickle Cell Disease: A Review. Immunohematology 2009, 25, 67–74. [PubMed: 19927623]

(4). Delaye M; Tardieu A Short-Range Order of Crystallin Proteins Accounts for Eye Lens Transparency. Nature 1983, 302, 302415a0.

(5). Huizinga A; Bot AC; de Mul FF; Vrensen GF; Greve J Local Variation in Absolute Water Content of Human and Rabbit Eye Lenses Measured by Raman Microspectroscopy. Experimental Eye Research 1989, 48, 487–496. [PubMed: 2714410]

(6). Lynnerup N; Kjeldsen H; Heegaard S; Jacobsen C; Heinemeier J Radiocarbon Dating of the Human Eye Lens Crystallines Reveal Proteins without Carbon Turnover throughout Life. PLoS ONE 2008, 3.

(7). Horwitz J Alpha-crystallin can function as a molecular chaperone. Proceedings of the National Academy of Sciences of the United States of America 1992, 89, 10449–10453. [PubMed: 1438232]

(8). Peschek J; Braun N; Franzmann TM; Georgalis Y; Haslbeck M; Weinkauf S; Buchner J The Eye Lens Chaperone a-Crystallin Forms Defined Globular Assemblies. Proceedings of the National Academy of Sciences 2009, 106, 13272–13277.

(9). Ma Z; Hanson SR; Lampi KJ; David LL; Smith DL; Smith JB Age-Related Changes in Human Lens Crystallins Identified by HPLC and Mass Spectrometry. Experimental Eye Research 1998, 67, 21–30. [PubMed: 9702175]

(10). Chaudhury S; Ghosh P; Parveen S; Dasgupta S Glycation of Human γB-Crystallin: A Biophysical Investigation. International Journal of Biological Macromolecules 2017, 96, 392–402. [PubMed: 28013006]

(11). Aquilina JA; Truscott RJW Identifying Sites of Attachment of UV Filters to Proteins in Older Human Lenses. Biochimica Et Biophysica Acta 2002, 1596, 6–15. [PubMed: 11983416]

(12). Litt M; Kramer P; LaMorticella DM; Murphey W; Lovrien EW; Weleber RG Autosomal Dominant Congenital Cataract Associated with a Missense Mutation in the Human Alpha Crystallin Gene CRYAA. Human Molecular Genetics 1998, 7, 471–474. [PubMed: 9467006]

(13). Mackay DS; Andley UP; Shiels A Cell Death Triggered by a Novel Mutation in the aA-Crystallin Gene Underlies Autosomal Dominant Cataract Linked to Chromosome 21q. European journal of human genetics: EJHG 2003, 11, 784–793. [PubMed: 14512969]

(14). Bova MP; Yaron O; Huang Q; Ding L; Haley DA; Stewart PL; Horwitz J Mutation R120G in aB-Crystallin, Which Is Linked to a Desmin-Related Myopathy, Results in an Irregular Structure and Defective Chaperone-like Function. Proceedings of the National Academy of Sciences of the United States of America 1999, 96, 6137–6142. [PubMed: 10339554]

(15). Vendra VPR; Khan I; Chandani S; Muniyandi A; Balasubramanian D γ Crystallins of the Human Eye Lens. Biochimica et Biophysica Acta (BBA) - General Subjects 2016, 1860, 333–343. [PubMed: 26116913]

(16). Boatz JC; Whitley MJ; Li M; Gronenborn AM; van der Wel PCA Cataract-Associated P23T γD-Crystallin Retains a Native-like Fold in Amorphous-Looking Aggregates Formed at Physiological pH. Nature Communications 2017, 8, 15137.

(17). Pande A; Zhang J; Banerjee PR; Puttamadappa SS; Shekhtman A; Pande J NMR Study of the Cataract-Linked P23T Mutant of Human γD-Crystallin Shows Minor Changes in Hydrophobic Patches That Reflect Its Retrograde Solubility. Biochemical and biophysical research communications 2009, 382, 196–199. [PubMed: 19275895]

(18). Jung J; Byeon I-JL; Wang Y; King J; Gronenborn AM The Structure of the Cataract-Causing P23T Mutant of Human γD-Crystallin Exhibits Distinctive Local Conformational and Dynamic Changes. Biochemistry 2009, 48, 2597–2609. [PubMed: 19216553]

(19). Ma Z; Piszczek G; Wingfield PT; Sergeev YV; Hejtmancik JF The G18V CRYGS Mutation Associated with Human Cataracts Increases γS-Crystallin Sensitivity to Thermal and Chemical Stress. Biochemistry 2009, 48, 7334–7341. [PubMed: 19558189]

(20). Vendra VPR; Chandani S; Balasubramanian D The Mutation V42M Distorts the Compact Packing of the Human γS-Crystallin Molecule, Resulting in Congenital Cataract. PLOS ONE 2012, 7, e51401. [PubMed: 23284690]

(21). Karri S; Kasetti RB; Vendra VPR; Chandani S; Balasubramanian D Structural Analysis of the Mutant Protein D26G of Human γS-Crystallin, Associated with Coppock Cataract. Molecular Vision 2013, 19, 1231–1237. [PubMed: 23761725]

(22). Kingsley CN; Brubaker WD; Markovic S; Diehl A; Brindley AJ; Oschkinat H; Martin RW Preferential and Specific Binding of Human aB-Crystallin to Cataract-Related Variant of γS-Crystallin. Structure (London, England : 1993) 2013, 21, 2221–2227.

(23). Brubaker WD; Freites JA; Golchert KJ; Shapiro RA; Morikis V; Tobias DJ; Martin RW Separating Instability from Aggregation Propensity in γS-Crystallin Variants. Biophysical Journal 2011, 100, 498–506. [PubMed: 21244846]

(24). Khago D; Wong EK; Kingsley CN; Freites JA; Tobias DJ; Martin RW Increased hydrophobic surface exposure in the cataract-related G18V variant of human γS-crystallin. Biochimica et Biophysica Acta (BBA)-General Subjects 2016, 1860, 325–332. [PubMed: 26459004]

(25). Mishra S; Stein RA; Mchaourab HS Cataract-Linked γD-Crystallin Mutants Have Weak Affinity to Lens Chaperones a-Crystallins. FEBS Letters 2012, 586, 330–336. [PubMed: 22289178]

(26). Zarina S; Slingsby C; Jaenicke R; Zaidi ZH; Driessen H; Srinivasan N Three-Dimensional Model and Quaternary Structure of the Human Eye Lens Protein Gamma S-Crystallin Based on Beta- and Gamma-Crystallin X-Ray Coordinates and Ultracentrifugation. Protein Science : A Publication of the Protein Society 1994, 3, 1840–1846. [PubMed: 7849599]

(27). Wang Y; Petty S; Trojanowski A; Knee K; Goulet D; Mukerji I; King J Formation of Amyloid Fibrils In Vitro from Partially Unfolded Intermediates of Human γC-Crystallin. Investigative Ophthalmology & Visual Science 2010, 51, 672–678. [PubMed: 19684009]

(28). Xu J; Chen J; Toptygin D; Tcherkasskaya O; Callis P; King J; Brand L; Knutson JR Femtosecond Fluorescence Spectra of Tryptophan in Human γ-Crystallin Mutants: Site-Dependent Ultrafast Quenching. Journal of the American Chemical Society 2009, 131, 16751–16757. [PubMed: 19919143]

(29). Chen J; Callis PR; King J Mechanism of the Very Efficient Quenching of Tryptophan Fluorescence in Human γD- and γS-Crystallins: The γ-Crystallin Fold May Have Evolved To Protect Tryptophan Residues from Ultraviolet Photodamage. Biochemistry 2009, 48, 3708–3716. [PubMed: 19358562]

(30). Kosinski-Collins MS; Flaugh SL; King J Probing folding and fluorescence quenching in human yD crystallin Greek key domains using triple tryptophan mutant proteins. Protein Science 2004, 13, 2223–2235. [PubMed: 15273315]

(31). Flaugh SL; Kosinski-Collins MS; King J Contributions of hydrophobic domain interface interactions to the folding and stability of human γD-crystallin. Protein Science 2005, 14, 569–581. [PubMed: 15722442]

(32). Pokalsky C; Wick P; Harms E; Lytle FE; Van Etten RL Fluorescence Resolution of the Intrinsic Tryptophan Residues of Bovine Protein Tyrosyl Phosphatase. The Journal of Biological Chemistry 1995, 270, 3809–3815. [PubMed: 7876123]

(33). Banerjee PR; Puttamadappa SS; Pande A; Shekhtman A; Pande J Increased Hydrophobicity and Decreased Backbone Flexibility Explain the Lower Solubility of a Cataract-Linked Mutant of γD-Crystallin. Journal of Molecular Biology 2011, 412, 647–659. [PubMed: 21827768]

(34). Pande A; Ghosh KS; Banerjee PR; Pande J Increase in Surface Hydrophobicity of the Cataract-Associated P23T Mutant of Human γD-Crystallin Is Responsible for Its Dramatically Lower, Retrograde Solubility. Biochemistry 2010, 49, 6122–6129. [PubMed: 20553008]

(35). Bothra A; Bhattacharyya A; Mukhopadhyay C; Bhattacharyya K; Roy S A Fluorescence Spectroscopic and Molecular Dynamics Study of Bis-ANS/Protein Interaction. Journal of Biomolecular Structure & Dynamics 1998, 15, 959–966. [PubMed: 9619517]

(36). Hawe A; Sutter M; Jiskoot W Extrinsic Fluorescent Dyes as Tools for Protein Characterization. Pharmaceutical Research 2008, 25, 1487–1499. [PubMed: 18172579]

(37). Bodenhausen G; Ruben D Natural abundance nitrogen-15 NMR by enhanced heteronuclear spectroscopy. Chemical Physics Letters 1980, 69, 185–189.

(38). Brubaker WD; Martin RW ^{1}H, ^{13}C, and ^{15}N Assignments of Wild-Type Human γS-Crystallin and Its Cataract-Related Variant γS-G18V. Biomolecular NMR Assignments 2012, 6, 63–67. [PubMed: 21735120]

(39). Greene RF; Pace CN Urea and Guanidine Hydrochloride Denaturation of Ribonuclease, Lysozyme, α-Chymotrypsin, and β-Lactoglobulin. Journal of Biological Chemistry 1974, 249, 5388–5393. [PubMed: 4416801]

(40). Delaglio F; Grzesiek S; Vuister GW; Zhu G; Pfeifer J; Bax A NMRPipe: A Multidimensional Spectral Processing System Based on UNIX Pipes. Journal of Biomolecular NMR 1995, 6, 277–293. [PubMed: 8520220]

(41). Lee W; Tonelli M; Markley JL NMRFAM-SPARKY: Enhanced Software for Biomolecular NMR Spectroscopy. Bioinformatics 2015, 31, 1325–1327. [PubMed: 25505092]

(42). Phillips JC; Braun R; Wang W; Gumbart J; Tajkhorshid E; Villa E; Chipot C; Skeel RD; Kale L; Schulten K Scalable molecular dynamics with NAMD. J Comp Chem 2005, 26, 1781–802. [PubMed: 16222654]

(43). Best RB; Mittal J; Feig M; MacKerell JAD, Inclusion of many-body effects in the additive CHARMM protein CMAP potential results in enhanced cooperativity of alpha-helix and beta-hairpin formation. Biophys J 2012, 103, 1045–51. [PubMed: 23009854]

(44). MacKerell JAD; Feig M; Brooks I,CL Extending the treatment of backbone energetics in protein force fields: Limitations of gas-phase quantum mechanics in reproducing conformational distributions in molecular dynamics simulations. J. Comput. Chem 2004, 25, 1400–1415. [PubMed: 15185334]

(45). MacKerell JAD, et al. All-atom empirical potential for molecular modeling and dynamics studies of proteins. J. Phys. Chem. B 1998, 102, 3586–3616. [PubMed: 24889800]

(46). Jorgensen W; Chandrasekhar J; Madura J; Impey R; Klein M Comparison of simple potential functions for simulating liquid water. J. Chem. Phys 1983 , 79, 926–935.

(47). Essmann U; Perera L; Berkowitz ML; Darden T; Lee H; Pedersen LG A smooth particle mesh Ewald method. The Journal of Chemical Physics 1995, 103, 8577–8593.

(48). Darden T; York D; Pedersen L Particle mesh Ewald: An N log(N) method for Ewald sums in large systems. The Journal of Chemical Physics 1993, 98, 10089–10092.

(49). Grubmuller H; Heller H; Windemuth A; Schulten K Generalized Verlet Algorithm for Efficient Molecular Dynamics Simulations with Long-range Interactions. Molecular Simulation 1991, 6, 121–142.

(50). Ryckaert J-P; Ciccotti G; Berendsen H Numerical integration of the Cartesian equations of motion of a system with constraints: Molecular dynamics of n-alkanes. Journal of Computational Physics 1977, 23, 327–341.

(51). Miyamoto S; Kollman PA Settle: An analytical version of the SHAKE and RATTLE algorithm for rigid water models. Journal of Computational Chemistry 1992, 13, 952–962.

(52). Martyna G; Tobias D; Klein M Constant-pressure molecular-dynamics algorithms. J. Chem. Phys 1994, 101, 4177–4189.

(53). Feller SE; Zhang Y; Pastor RW; Brooks BR Constant pressure molecular dynamics simulation: The Langevin piston method. The Journal of Chemical Physics 1995, 103, 4613–4621.

(54). Kabsch W; Sander C Dictionary of Protein Secondary Structure: Pattern Recognition of Hydrogen-Bonded and Geometrical Features. Biopolymers 1983, 22, 2577–2637. [PubMed: 6667333]

(55). Joosten RP; te Beek TA; Krieger E; Hekkelman ML; Hooft RW; Schneider R; Sander C; Vriend G A Series of PDB Related Databases for Everyday Needs. Nucleic Acids Research 2011, 39, D411–D419. [PubMed: 21071423]
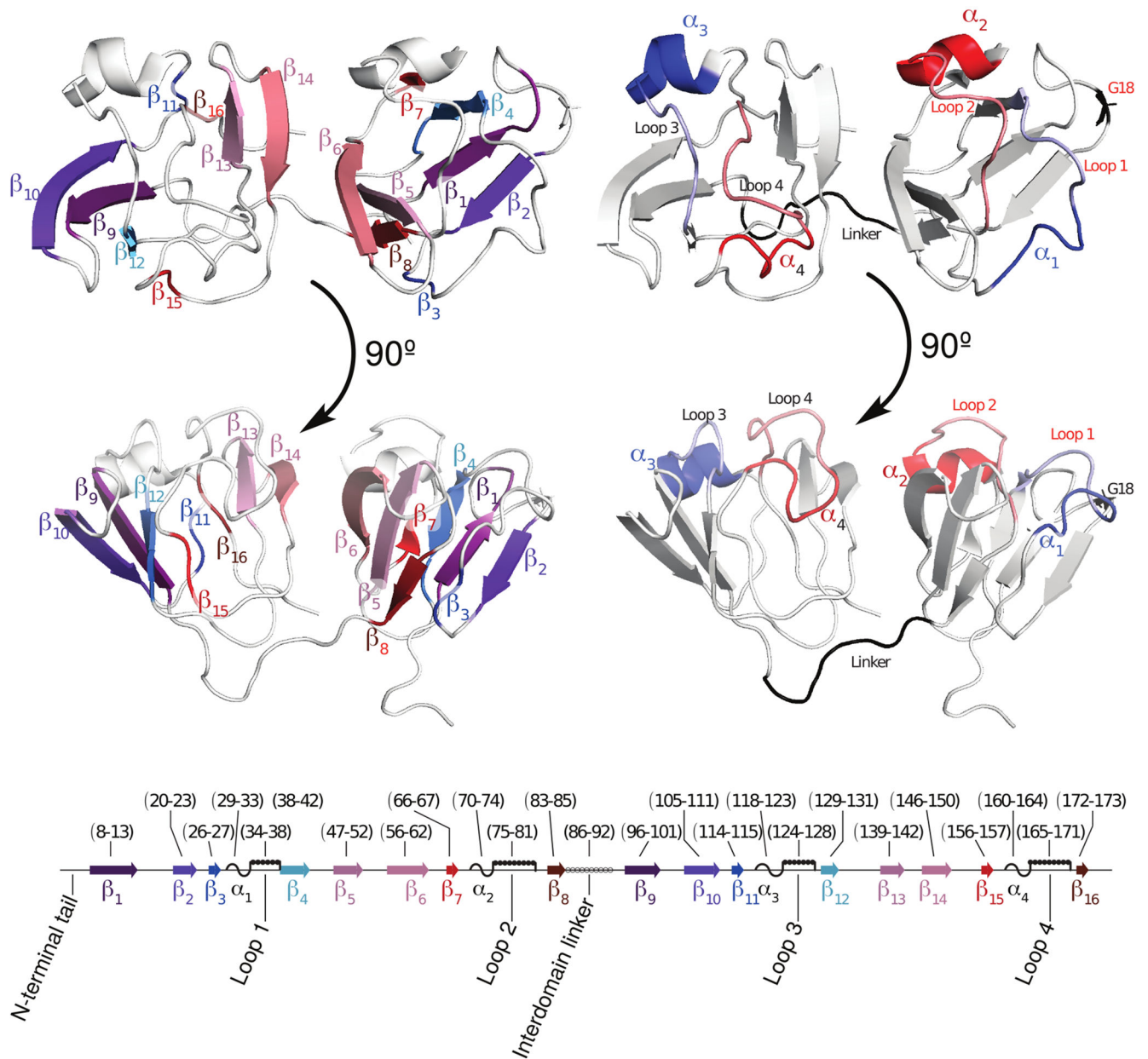
Figure 1:

A schematic view of human γS-WT (PDB ID: 2M3T), highlighting key sequence features, including β-strands (Left) and α-helices or loops (Right) on the structure. The mutated residue (G18) is labeled as well. The span of each helix, strand, or loop is laid out linearly (Bottom) to indicate how the sequence of γS-WT relates to the structure.
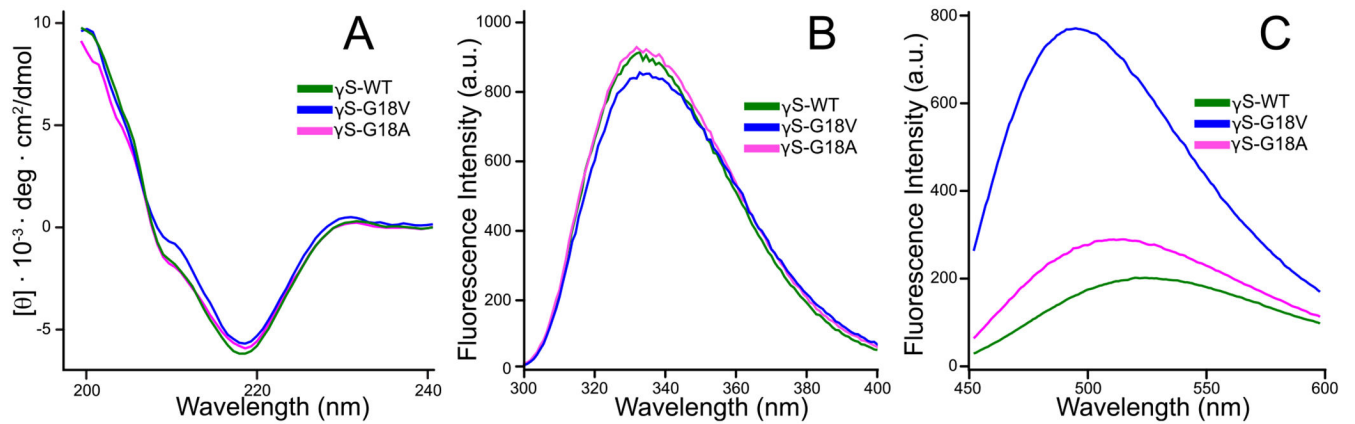
Figure 2:
CD spectra indicate that the overall fold of γS-G18A is similar to that of γS-WT. (**A**) CD spectra of γS-WT, γS-G18A, and γS-G18V. The spectra of all three proteins are similar overall, however γS-G18V has a shoulder at 200-210 nm not observed in the others. (**B**) Intrinsic tryptophan fluorescence spectra of γS-WT, γS-G18A, and γS-G18V after excitation at 280 nm. The spectrum of the γS-G18V variant exhibits a slight red shift relative to the other two. (**C**) ANS binding assay for γS-WT, γS-G18A, and γS-G18V. The γS-G18V variant has the highest intensity, indicating that the γS-G18V variant has the largest hydrophobic surface area exposed to solvent.
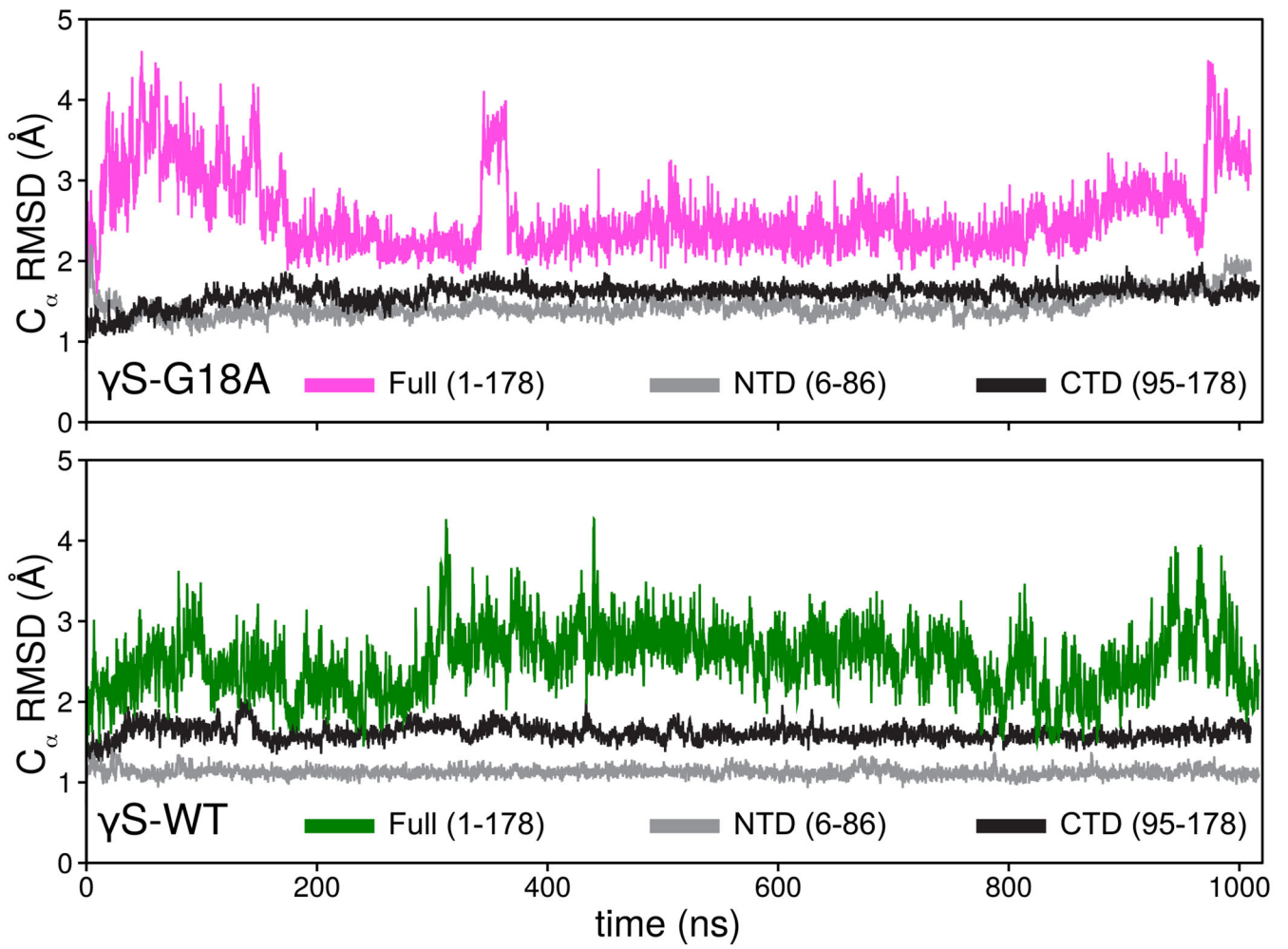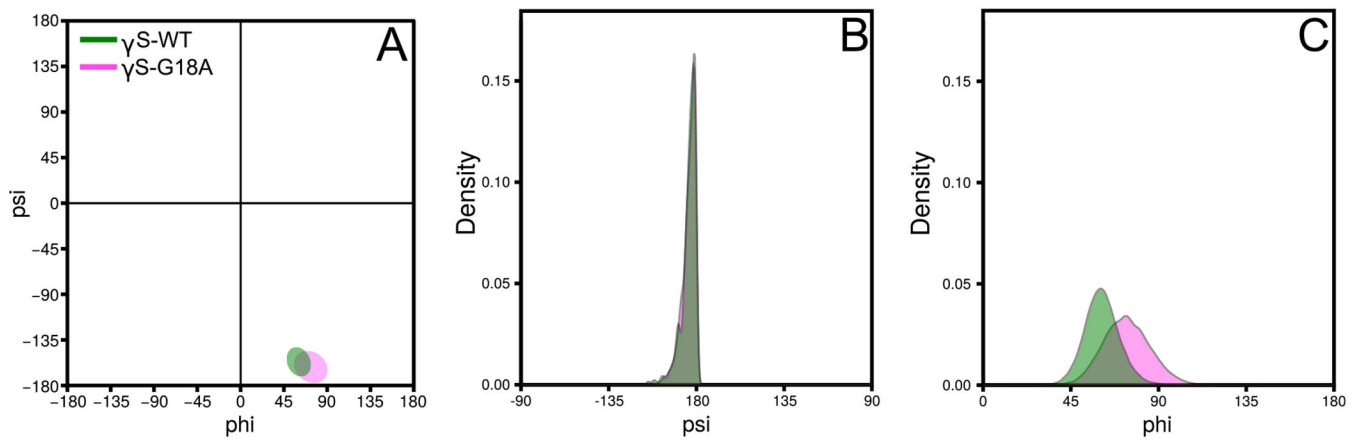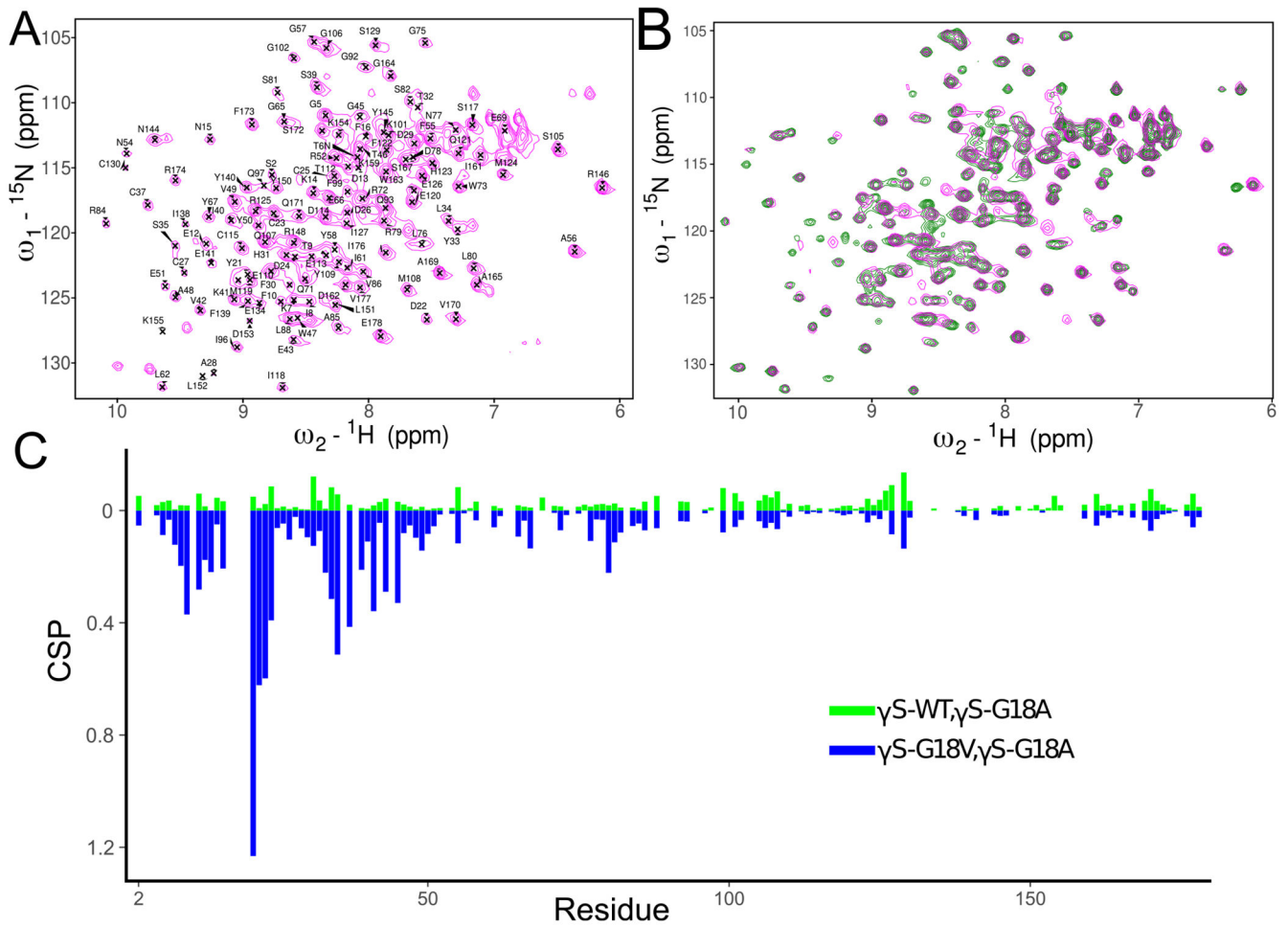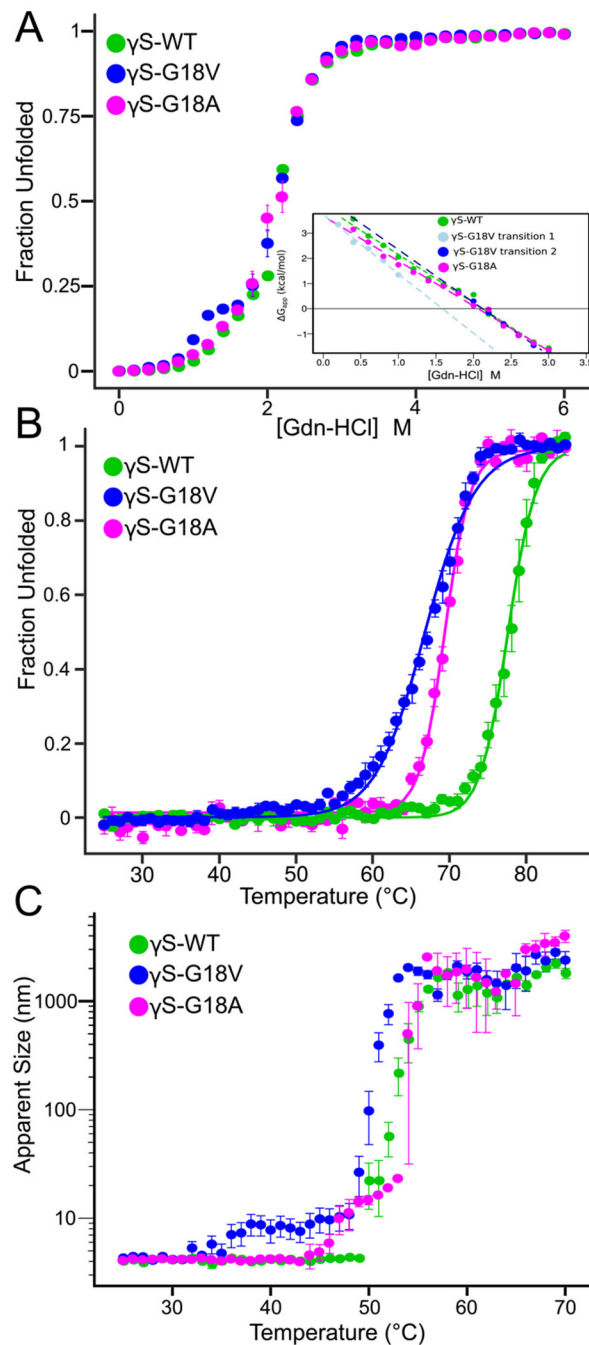
Figure 3:
C_a RMSD from the initial configuration. The time evolution of γS-G18A predicts a well-folded protein much like γS-WT. Full = RMSD of all a-carbons. CTD = RMSD of residues 95-178. NTD = RMSD of residues 6-86.

Figure 4:
Backbone torsion angles for lens γS-crystallin residue 18. (**A**) The ψ-φ populations of γS-G18A are similar to those of γS-WT. (**B**) The ψ torsion angle distributions are almost identical, while (**C**) the γS-G18A φ torsional angle distribution is broader that in γS-WT.

Figure 5:
(**A**) ^{1}H-^{15}N HSQC spectrum of γS-G18A. Peaks were assigned by comparing the spectrum of γS-G18A to the previously assigned spectra of γS-WT and γS-G18V.[38] (**B**) Overlaid ^{1}H-^{15}N HSQC spectra of γS-WT (green) and γS-G18A (magenta). The two spectra overlay very well but some peaks are in slightly different positions. (**C**) Comparison of the chemical shift differences between γS-G18A and γS-WT (green) and γS-G18A to γS-G18V (blue).

Figure 6:

The stability and aggregation propensity of γS-G18A are more similar to γS-WT than to γS-G18V, although decreased stability is observed. (**A**) Chemical stability of γS-WT, γS-G18A, and γS-G18V was measured by taking the ratio of 355/325 nm after incubation in increasing concentrations of guanidine hydrochloride. Both γS-WT and γS-G18A show very similar results. However, γS-G18V is the least stable protein, exhibiting a three-stage unfolding pattern. The inset shows the linear extrapolation used to calculate the parameters in Table 1. (**B**) Thermal unfolding curves were generated by monitoring the CD intensity at

218 nm as a function of temperature for γS-WT (green), γS-G18A (magenta), and γS-G18V (blue). γS-WT is the most stable protein with a thermal unfolding midpoint temperature (T_m) of 77.67±0.03 °C. The γS-G18A variant is of intermediate stability, with a T_m of 69.87±0.05 °C, while the γS-G18V variant is the least stable with a T_m of 66.74±0.04 °C. (**C**) Thermal aggregation propensity was measured by DLS. Both γS-G18A and γS-G18V are aggregation-prone relative to wild-type, however, γS-G18V forms small aggregates at physiological temperature, where γS-G18A remains monomeric. Each experiment was repeated three times.

Figure 7:
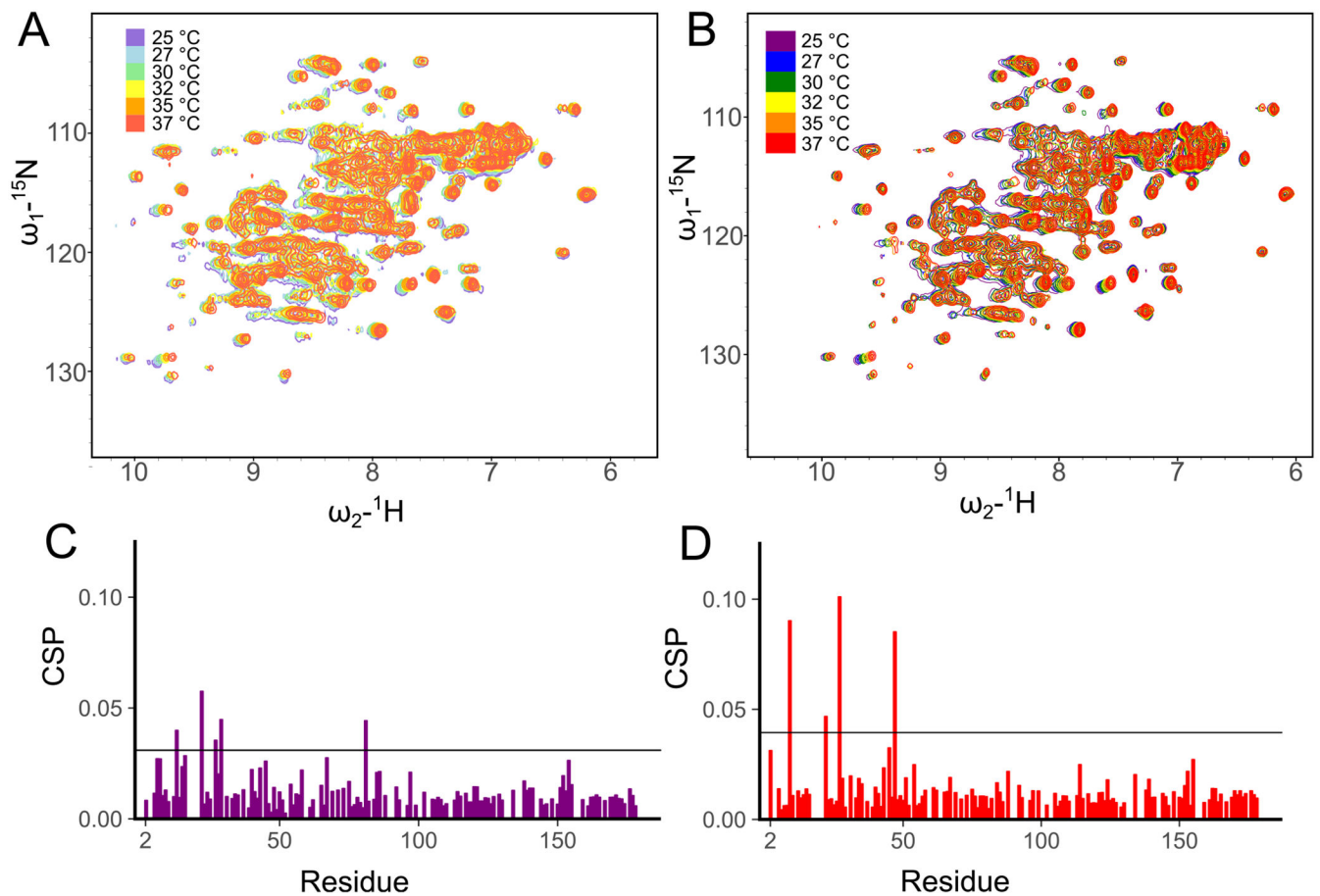
αB-crystallin does not specifically bind γS-G18A. (**A**) ^{15}N-HSQC spectra of ^{15}N-labeled γS-G18A as a function of temperature. (**B**) ^{15}N-HSQC spectra of ^{15}N-labeled γS-G18A mixed with natural abundance αB-crystallin. The spectra are almost identical, suggesting little interaction between γS-G18A and αB. (**C**) Observed CSPs for γS-G18A compared to γS-G18A+αB at 25 °C indicate very little change in conformation, suggesting minimal interaction. Only four residues have a CSP greater than 2 * *RMS*, residues 13, 22, 29, and 81. (**D**) a similar observation is made at 37 °C where only four residues show a CSP greater than 2 * *RMS*, these residues are 9, 22, 27, and 47.
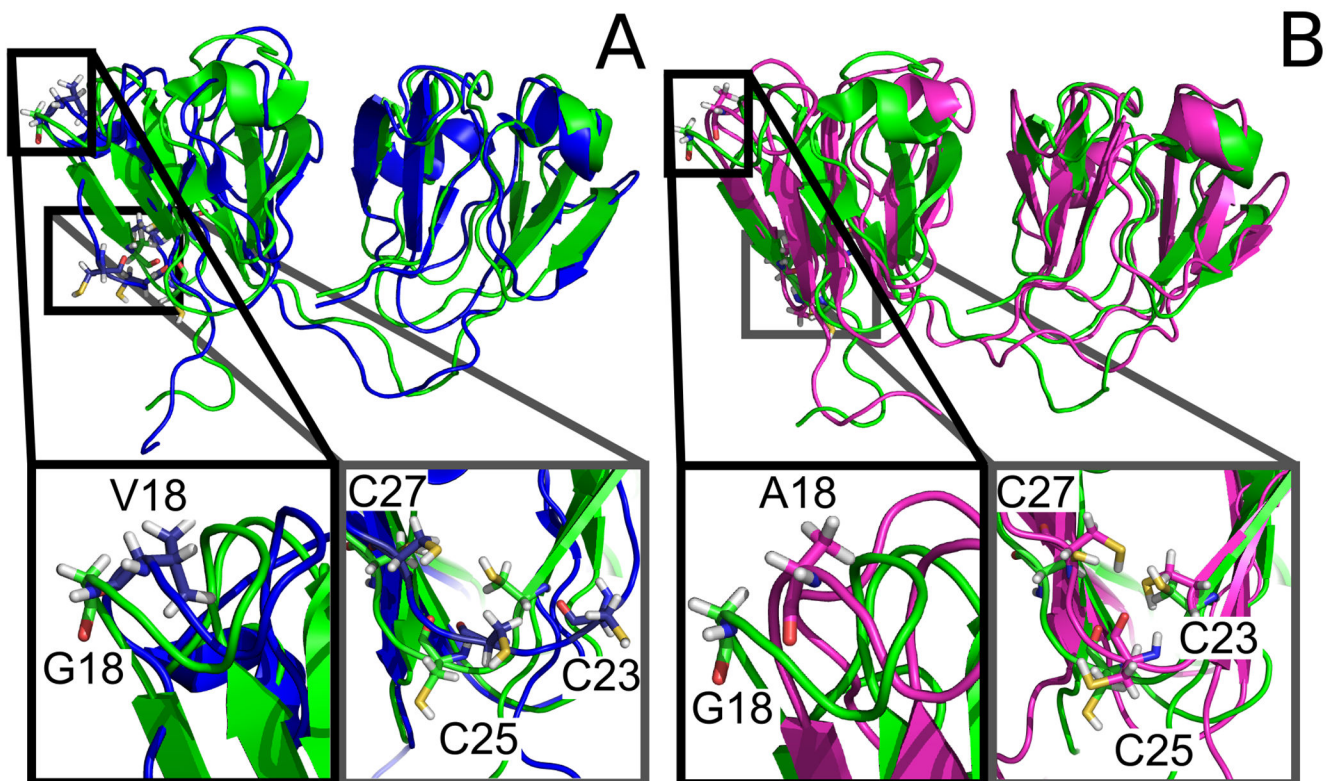
Figure 8:

The predicted structure of γS-G18A is very similar to that of γS-WT. (**A**) The overall structures of γS-WT (PDB ID: 2M3T) and γS-G18V (PDBID: 2M3U) are very similar but there are some key differences. The loop region around the mutation site exhibits an altered conformation suggesting altered salt-bridging interactions with this loop region. The cysteine residues in γS-G18V are pointed out into the solvent and not turned into the protein like in γS-WT. (**B**) Comparing a predicted structure of γS-G18A generated from molecular dynamics simulations to the NMR structure of γS-WT shows some important similarities. Although γS-G18A has a slightly altered conformation in the loop region around the mutation site, the disturbances are not sufficient enough to alter the conformation of the loop containing cysteines 23, 25 and 27, in contrast to γS-G18V, where these cysteines are more exposed to solvent.

Table 1:

Thermodynamic parameters as calculated from chemical unfolding in Gnd-HCl. The midpoint of unfolding is similar for all three proteins in the final transition, but γS-G18V shows a stable intermediate. The parameters were calculated from the lines shown in Supplementary Figure S4 where "m" represents the slope of each line. The midpoint of unfolding was read at the x-intercept for each line and ΔG$_{app}$ was read at the y-intercept

	Transition 1			Transition 2		
Protein	Midpoint [Gnd-HCl]	G$_{app}$(kcal/mol)	m (kcal·mol^{-1}·M^{-1})	Midpoint [Gnd-HCl]	G$_{app}$(kcal/mol)	m (kcal·mol^{-1}·M^{-1})
WT				2.14±0.01 M	4.07±0.01	−1.93±0.01
G18V	1.58±0.01 M	3.73±0.1	−2.36±0.01	2.3 M±0.01	4.43±0.01	−2.14± 0.01
G18A				2.11±0.01 M	3.68±0.01	−1.75±0.01